Data Assimilation for Streamflow Forecasting: State–Parameter Assimilation versus Output Assimilation

Leqiang Sun, Ph.D.[1]; Ousmane Seidou[2]; and Ioan Nistor[3]

Abstract: This paper compares two data assimilation methods: state–parameter assimilation and output assimilation in improving streamflow forecasting using the Soil and Water Assessment Tool (SWAT) model. The state–parameter assimilation is performed by updating the stored water content and soil curve number with the extended Kalman filter (EKF); the output assimilation is carried out by updating the model output errors with autoregressive (AR) models. The performances of the two data assimilation techniques are compared for a dry year and a wet year, and it is found that whereas both methods significantly improve forecasting accuracy, their performances are influenced by the hydrological regime of the particular year. During the wet year, the average root-mean-square error (RMSE) for seven days forecasts is improved from 670.46 to 420.42 m^3/s when output assimilation is used, and to 367.60 m^3/s when state–parameter assimilation is used. The Nash–Sutcliffe coefficient (NSC) is improved from 0.63 to 0.85 and 0.88, respectively; the mean error (ME) is improved from -375.83 m^3/s to -131.68 m^3/s and -129.11 m^3/s, respectively. For shorter forecast leads (1–4 days), the state–parameter assimilation outperforms output assimilation in both dry and wet years. For longer forecast leads (5–7 days), the output assimilation could provide better results in the wet year. A hybrid method that combines state–parameter assimilation and output assimilation performs very well in both dry and wet years according to all three indicators. **DOI: 10.1061/(ASCE)HE.1943-5584.0001475.** © *2016 American Society of Civil Engineers.*

Author keywords: Data assimilation; Streamflow forecast; Soil and Water Assessment Tool (SWAT); Extended Kalman filter; Autoregressive model.

Introduction

Streamflow forecasting can be performed with either stochastic or physically based models. Stochastic models are data-driven and usually simple to implement, but they lack connection with the real world (Todini 1988, 2007). Physically based models have stronger physical rationality but do not necessarily generate more accurate forecasts than stochastic models (Anctil et al. 2004; Zealand et al. 1999) because of the additional uncertainty in inputs, parameterization, and model structure (Beven 1989).

A method that involves both deterministic and stochastic components could benefit the robustness of the former and the adaptability of the latter (Todini 2007). Examples of such approaches include probabilistic forecasting (Krzysztofowicz 1999, 2001), combined forecasting (Chen et al. 2015; Jeong and Kim 2009), and ensemble forecasting (Cloke and Pappenberger 2009; Velázquez et al. 2011). In these approaches, the deterministic models are typically applied under a statistical framework (Ajami et al. 2007; Georgakakos et al. 2004). Challenges in such approaches include computational burden and outputs that are less intuitive for decision makers when they are used in an operational setting (Ajami et al. 2007; Cloke and Pappenberger 2009; De Kleermaeker and Verkade 2013).

Data assimilation (DA) is a method that combines the strengths of the deterministic model and statistical estimation methods by integrating the most recent observations into model outputs (Kitanidis and Bras 1980b; Vrugt et al. 2006). DA is easier to implement because it normally only requires one model and minimum historical observations. In a broad sense, DA includes input assimilation (Chen et al. 2014; Massari et al. 2014), state–parameter assimilation (Hendricks Franssen and Kinzelbach 2008; Lü et al. 2011; Moradkhani et al. 2005b; Vrugt et al. 2005), and output assimilation (Anctil et al. 2003; Broersen 2007; Sene 2008; Yu and Chen 2005).

State and parameter DA has experienced rapid development since the 1990s. This type of DA can be divided into objective methods and sequential methods. Compared to objective methods, sequential methods are capable of handling all sources of uncertainty (Moradkhani 2008) and are less complex to implement. Sequential methods that are commonly used in hydrologic DA include the use of particle filter (Moradkhani et al. 2005a; Pham 2001; Weerts and El Serafy 2006), H-infinity filter (Lü et al. 2010; Wang and Cai 2008), linear Kalman filter (Kalman 1960) and its heirs like the extended Kalman filter (EKF) (Puente and Bras 1987), the ensemble Kalman filter (EnKF) (Evensen 1994), the unscented Kalman filter (UKF) (Wan and Van Der Merwe 2000), and so forth.

Theoretically, the extended Kalman filter (EKF) is the standard method to expand the linear Kalman filter to nonlinear systems.

[1]Dept. of Civil Engineering, Faculty of Engineering, Univ. of Ottawa, 161, Louis Pasteur St., Ottawa, ON, Canada K1N 6N5 (corresponding author). ORCID: http://orcid.org/0000-0002-0842-2262. E-mail: lsun034@uottawa.ca

[2]Associate Professor, Dept. of Civil Engineering, Faculty of Engineering, Univ. of Ottawa, 161, Louis Pasteur St., Ottawa, ON, Canada K1N 6N5.

[3]Professor, Dept. of Civil Engineering, Faculty of Engineering, Univ. of Ottawa, 161, Louis Pasteur St., Ottawa, ON, Canada K1N 6N5.

Note. This manuscript was submitted on November 12, 2015; approved on August 5, 2016; published online on October 12, 2016. Discussion period open until March 12, 2017; separate discussions must be submitted for individual papers. This paper is part of the ***Journal of Hydrologic Engineering***, © ASCE, ISSN 1084-0699.

If done properly, the implementation of EKF is neat and straightforward. However, because of the complexity of the linearization of the nonlinear hydrological model, this method has rarely been used in hydrological DA, especially in the case of distributed models (Kitanidis and Bras 1980b; Walker and Houser 2001).

Output assimilation (also known as error update or error assimilation) is fundamentally different from state–parameter assimilation. In typical output assimilation, a stochastic model is calibrated using the historical model output error, and the improved forecast is calculated by adding the predicted error to the initial model forecast. Examples of stochastic models used in output assimilation include: autoregressive moving average (ARMA) models (Angela 1982; Broersen 2007; Chen et al. 2015; Wu et al. 2012), artificial neural networks (ANNs) (Anctil et al. 2003; Jain and Srinivasulu 2004; Jeevaragagam and Simonovic 2013; Khac-Tien Nguyen and Hock-Chye Chua 2012), *dual pass* method (Pagano et al. 2011), hybrid methods that combine ARMA or ANNs with Kalman filters (Bidwell and Griffiths 1994; Muluye 2011), and so forth. Xiong and O'Connor (2002) compared the AR model with other more complicated models and found that the latter do not necessarily outperform the standard AR model.

Output assimilation methods are independent of the structure and parameters of deterministic models, and hence they are usually more efficient to apply. The deterministic models do not receive any feedback from the error update, but only generate more error samples into the training pool if the update is carried online (Tingsanchali and Gautam 2000). Compared to state–parameter assimilation methods, output assimilation methods are incapable of handling uncertainty in the observation, and neither can they improve the deterministic models' structures and parameters. For this reason, output assimilation is found more effective than the deterministic models in open-loop mode for shorter-range forecasting (Angela 1982).

Madsen and Skotner (2005) described a combined state and output assimilation scheme in real-time flood forecasting with the MIKE 11 model. The state update procedure was used in the hydrodynamic module, and the error forecasting was implemented with a second-order autoregressive model. Bauer-Gottwein et al. (2015) applied the standard linear Kalman filter for the state update of the Muskingum routing model in the Soil and Water Assessment Tool (SWAT) model. Both of these two studies only focus on the hydrodynamic module of the deterministic models. There is a growing consensus in the literature (Berg and Mulroy 2006; Berthet et al. 2009; Brocca et al. 2009; Javelle et al. 2010; McMillan et al. 2013) that the update of the initial conditions of the watershed, especially the antecedent moisture content (AMC), has great potential in the enhancement of streamflow forecasting. Hybrid assimilation of the rainfall runoff module may improve longer-range forecasting, but such research is rare to the authors' knowledge (Bauer-Gottwein et al. 2015).

The aim of this paper is to compare the effectiveness of state–parameter assimilation and output assimilation in improving the forecasting abilities of the SWAT model (Arnold et al. 1998). For state–parameter assimilation, EKF is used to assimilate the measured streamflow into the simulation of the watershed runoff. For output assimilation, AR models are applied to predict model errors. Additionally, a hybrid method is suggested to couple the EKF assimilation results with an AR model in updating the SWAT model errors. The remainder of the paper is organized as follows: the next section introduces the methodology; the third section introduces the SWAT model and the research area; the section on EKF state assimilation explains the experimental design details, including the implementation of state–parameter assimilation with EKF and the output assimilation with the AR model; the results and analysis are presented in the fifth section; and the conclusions are given in the final section.

Extended Kalman Filter and ARMA Model

Extended Kalman Filter

The Kalman filter is an optimal estimator that recursively couples observations into a linear model to update the model states (Kalman 1960). The Kalman filter can only be applied to linear systems where both the dynamic and observation functions are linear. EKF was developed to deal with a nonlinear system, which can be represented by the state-space functions:

$$x_k^f = M_k(x_{k-1}^a, u_k, \eta_k) \tag{1}$$

$$\mathrm{y}_k^o = H_k(x_k^f, \varepsilon_k) \tag{2}$$

where M_k = dynamic model function; H_k = observation function; x_{k-1}^a = a posteriori state vector; and x_k^f = a priori state; u_k = *forcing* term; η_k = model error whose covariance matrix is termed Q_k; and y_k^o = observation with error ε_k, whose covariance matrix is R_k.

EKF requires the nonlinear system to be continuously derivable. It uses the first-order derivative of the Taylor extension at an estimated point to represent the nonlinear equation. The linearized model function and observation function are given as Eqs. (3) and (4):

$$M_k' = \left.\frac{\partial M_k}{\partial x_k}\right|_{(x_{k-1}^a, u_k, 0)} \tag{3}$$

$$H_k' = \left.\frac{\partial H_k}{\partial x_k}\right|_{(x_k^f, 0)} \tag{4}$$

For a model function $M = (M_1, M_2, \ldots, M_m)$ and a state vector $x = (x_1, x_2, \ldots, x_m)$, the linearized matrix is calculated with a Jacobian matrix as Eq. (5):

$$J_M = \begin{bmatrix} \frac{\partial M_1}{\partial x_1} & \cdots & \frac{\partial M_1}{\partial x_n} \\ \vdots & \ddots & \vdots \\ \frac{\partial M_m}{\partial x_1} & \cdots & \frac{\partial M_m}{\partial x_n} \end{bmatrix} \tag{5}$$

Eq. (5) is calculated numerically by perturbing the states of the model.

When the model and observation functions are replaced with their linearized versions M_k' and H_k', respectively, the EKF formulation can be expressed as:

- Step 1: propagation of the state:

$$x_k^f = M_k' x_{k-1}^a \tag{6}$$

- Step 2: propagation of the estimation error:

$$P_k^f = M_k' P_{k-1}^a M_k'^T + Q_k \tag{7}$$

In the preceding equations, the superscript a represents a posteriori estimation and the superscript f means a priori estimation. Q_k is the model error covariance matrix.

- Step 3: updating the a priori state estimate:

$$x_k^a = x_k^f + K_k \cdot v_k \tag{8}$$

in which $v_k = y_k^o - H_k' x_k^f$ is the innovation.

- Step 4: computing the Kalman gain:

$$K_k = P_k^f H_k'^T (R_k + H_k' P_k^f H_k'^T)^{-1} \tag{9}$$

where R_k = observation error covariance matrix.

- Step 5: updating the estimate error:

$$P_k^a = (I - K_k H_k') P_k^f \tag{10}$$

where I = unit matrix with the same dimension of $K_k H_k'$. Steps 1–5 are repeated to start another assimilation process whenever a new observation is available.

ARMA Models

It is well acknowledged that a stationary stochastic process can be approximated by a suitable autoregressive moving average (ARMA) model (Bidwell and Griffiths 1994; Choi 2012). Given a time series x, an ARMA model of orders p and q can be described by:

$$x_t + a_1 x_{t-1} + \cdots + a_p x_{t-p} = \varepsilon_t + b_1 \varepsilon_{t-1} + \cdots + b_q \varepsilon_{t-q} \tag{11}$$

where $a_1, \ldots, a_p$, and $b_1, \ldots, b_q$ are parameters; and $\varepsilon_t, \ldots, \varepsilon_{t-q}$ are white noise. The ARMA model degenerates into an AR model if $q = 0$ and an MA model if $p = 0$. The determination procedure of the orders and parameters of the ARMA model is well established by the Box–Jenkins method (Box and Jenkins 1976). Despite the fact that higher orders generally lead to more accurate forecast results, lower orders are found to be sufficient and more applicable for short-term forecasting (Broersen and Weerts 2005; Wu et al. 2012).

In order to obtain superior forecast accuracy, the following aspects should be considered: data selection, principal components, cross-validation,nd the optimal combination of independent variables (Garen 1992). In more advanced cases, complicated methods such as stepwise regression can be used to select and evaluate the order of importance of the predictors (Berger and Entekhabi 2001; Ssegane et al. 2012). The AR model normally only involves the time series of one variable. In this paper, the performance of multivariable AR models is compared with that of single-variable models. Although multivariable models violate the definition of an AR model, such examination may help to determine an optimal model that is more effective and robust.

SWAT Model

Model Structure

The Soil and Water Assessment Tools (SWAT) model is a semi-distributed conceptual hydrological model (Arnold et al. 1998; Jayakrishnan et al. 2005; Srinivasan et al. 1998). In the SWAT model, the hydrological processes are first simulated within the hydrological response units (HRUs), each of which features a unique combination of land-use, management, and soil types before they are lumped into subbasins. The runoff from the subbasins then joins the main channel and goes through a routing process before finally reaching the outlet of the watershed.

The hydrology component of SWAT is based on the water balance equation (Arnold et al. 1998):

$$SW_t = SW + \sum_{i=1}^{t} (R_i - Q_i - ET_i - P_i - QR_i) \tag{12}$$

where SW_t (mm) = soil water content at day t; SW (mm) = initial soil water content; R_i (mm) = daily precipitation; Q_i (mm) = daily runoff; ET_i (mm) = daily evapotranspiration; P_i (mm) = daily percolation; and QR_i (mm) = daily return flow.

The runoff consists of three parts: surface runoff, lateral runoff, and groundwater runoff. The surface runoff volume is calculated with a soil conservation service (SCS) curve number equation (Jacobs et al. 2003):

$$Q = \frac{(R - 0.2S)^2}{R + 0.8S}, \quad R > 0.2S \qquad Q = 0, \quad R \le 0.2S \tag{13}$$

where Q (mm) = daily surface runoff; R (mm) = daily rainfall; and S = retention parameter determined by the curve number (CN) with the SCS equation:

$$S = 254\left(\frac{100}{\mathrm{CN}} - 1\right) \tag{14}$$

The curve number is a function of soil permeability, land use, and antecedent soil water conditions. The curve number calculated on conditions of average antecedent soil water is termed CN2. The value of CN2 normally varies between 30 and 100. The curve numbers for dry and moist antecedent soil water conditions, CN1 and CN3, are calculated based on CN2. The calibration of CN2 is critical in SWAT. Once defined, it is used throughout the simulation until a new parameter CNOP is redefined in the subsequent operation processes.

The retention parameter S is tuned based on Eq. (15) (Arnold et al. 1998):

$$S = S_1 \left\{ 1 - \frac{\mathrm{FFC}}{\mathrm{FFC} + \exp[w_1 - w_2(\mathrm{FFC})]} \right\} \tag{15}$$

where S_1 = theoretical value calculated with CN1; FFC = fraction of field capacity, which is a function of soil water content SW (mm) and field capacity water content FC (mm); and w_1 and w_2 = shape parameters.

The actual daily curve number is then updated as:

$$\mathrm{DailyCN} = \frac{25{,}400}{(S + 254)} \tag{16}$$

Study Area

The SWAT model is developed for the watershed of the Bakel Hydrometric Station on the Senegal River in Senegal (Fig. 1). The watershed has an area of 420,546 km^2. The streamflow at Bakel Station is characterized by eight months of low flows (November–June) but unpredictably large floods in the rainy season, from July to October (S. Rimkus, "Performance measuring in the case of the Senegal River watershed management," working paper, ETH Zürich, Zürich, Switzerland). Given that streamflow observations are available at three interior stations (Gourbassi, Manantali, and Oualia) on the southern tributaries (Table 1), these stations (marked *Inlet* in Fig. 1) are treated as point inputs to the SWAT model. By such implementation, the SWAT model becomes a nonlinear input/output model, and the state update is only applied to the shaded area in Fig. 1. Subbasins upstream of locations with measured flow are not part of the area simulated with SWAT, and EKF is applied to the remainder of the watershed (shaded area in Fig. 1). For the sake of simplicity, errors in streamflow observations of these three interior stations are not considered explicitly in the implementation of EKF.

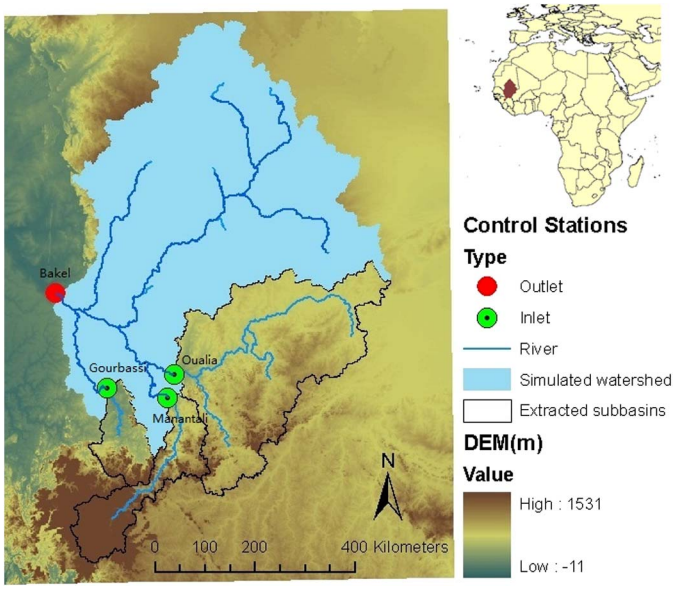

Fig. 1 Senegal River Watershed above Bakel Station

Table 1. Statistics of the Streamflow Observations (1988–2006) for Bakel and the Three Interior Stations

Stations	Mean (m^3/s)	Standard error (m^3/s)	Cs	Cv
Oualia	77	41	1.03	0.54
Gourbassi	76	31	0.65	0.41
Manantali	214	77	1.22	0.36
Bakel	446	167	1.12	0.37

Note: Cs = coefficient of skewness; Cv = coefficient of variation.

Table 2. SWAT Parameters Calibration Results (1990–1998)

Parameter	Initial lower limit	Initial upper limit	Calibrated lower limit	Calibrated upper limit	Fitted value
r__CN2.mgt[a]	−0.3	0.3	−0.03	0.04	0
v__ALPHA_BF.gw	0	1	0.44	0.81	0.62
v__GW_DELAY.gw	20	450	381.63	532.98	457.3
v__GWQMN.gw	0	500	514.29	670.91	592.6
v__GW_REVAP.gw	0	0.2	0.03	0.07	0.05
r__SOL_AWC(1).sol	−0.1	0.5	−0.02	0.29	0.14
r__SOL_K(1).sol	−0.2	0.8	0.16	0.36	0.26
r__SOL_BD(1).sol	−0.2	0.8	0.94	1.32	1.13
r__RCHRG_DP.gw	−0.2	0.2	0.13	0.23	0.18
r__SOL_Z(1).sol	−0.2	1	0.31	0.56	0.44
v__REVAPMN.gw	0	100	7.34	49.31	28.32
v__ALPHA_BNK.rte	0	1	0.47	0.82	0.65

[a]The prefix "r" means "relative" and "v" means "replace."

Calibration was done by comparing the simulated flow (surface runoff and base flow) to observations. The calibrated parameters can be found in Table 2 and Sun et al. (2015). The comparison between calibrated streamflow simulation from 1995 to 1998 and the validation in 1999 is shown in Fig. 2, and their statistic results [Eqs. (22)–(24)] are shown in Table 3. In general, SWAT provides a decent overall simulation for both wet and dry years but misses the flood peak in the extremely wet year of 1999.

The streamflow predictions for one-day to seven-day leads in 1992 and 1999 are evaluated. The RMSE and ME presented in the assessment of forecast improvement due to data assimilation are used to measure the difference between improved forecasts (rather than calibration and validation) and observations. 1992 was a relatively dry year for which the SWAT performs well. 1999 was a particularly wet year, and the performance of the SWAT simulation was lower than average. The comparison of the model's performance in these two representative years reveals the effectiveness of the assimilation methods in different hydrological regimes. Nevertheless, the results should be interpreted objectively, and more case studies are required for the generalization of these conclusions.

EKF State Assimilation and ARMA Output Assimilation

EKF State Assimilation and Forecast Assessment

Hydrological DA allows for a lot of flexibility in the selection of state variables. The water storage variables are the most commonly considered ones (Clark et al. 2008; Samuel et al. 2014). SWAT is usually operated with a daily time step; however, the water generated from HRUs may take more than one day to reach the channel. To handle this issue, SWAT divides the surface, lateral, and ground water runoff into two classifications: water that reaches the channel in the current day and lagged water, which takes more than one day to reach the channel. In this study, three intermediate water storage variables in the state vector are chosen based on trial and error: soil water content of the full soil profile, lagged surface runoff, and lagged lateral runoff.

Besides the water storage variables, it is often beneficial to update the model parameters in the hydrological DA (Lü et al. 2011; Moradkhani et al. 2005a). In EKF, the parameters can be augmented in the state vector. In this paper, only CN2 is selected because it is not only critical to the runoff simulation but is also found to be the most sensitive parameter affecting the simulation results.

The streamflow simulated by SWAT is also placed in the state vector. This way, the linear observation operator would be a vector whose element is 1 with regard to the streamflow, and zeroes for the rest (Evensen 1994). Hence, the final state vector contains the model output of streamflow, the three intermediate water storage variables—soil moisture, lagged surface runoff, and lagged lateral runoff—as well as the curve number CN2. The observation operator is simply a linear vector of (1, 0, 0, 0, 0).

Ratio Update Method

One of the issues in the implementation of EKF in distributed models is horizontal correlation of the distributed variables. Stacking all the distributed variables in the state vector would lead to an exceptionally large dimension of the state vector. In this study, only the watershed average value of a given variable or parameter is included in the state vector. The update of the variable or parameter at the HRU level is then accomplished using a *correction ratio* defined as:

$$\text{Ratio}\,(i) = \frac{x_k^a(i)}{x_k^f(i)} \tag{17}$$

where $x_k^a(i) = i$th element of the a posteriori state vector; and $x_k^f(i) = i$th element of the a priori state. Once the watershed scale ratio for a variable or parameter is calculated, the same variables on the HRU scale are all updated with the same ratio. Compared to the adding or replacing methods, the ratio method maintains the maximum spatial heterogeneity of the original distributed variables and parameters. Notice that the simulated streamflow is not a distributed variable and hence is not updated using this method.

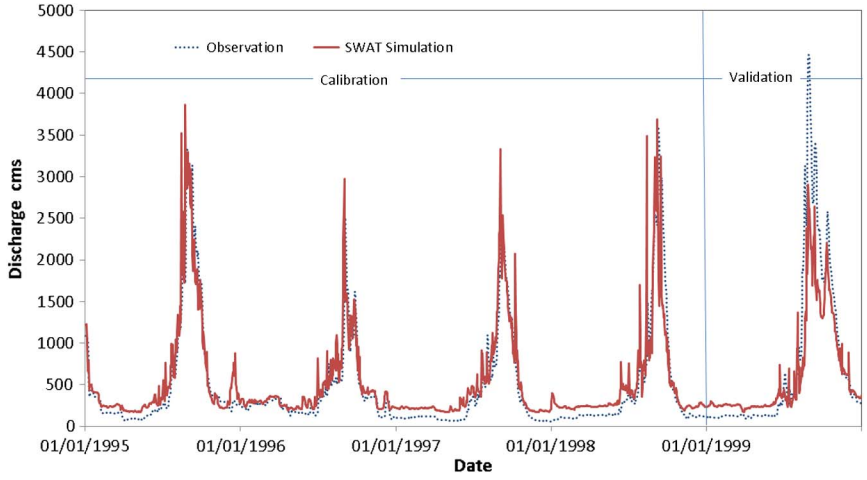

Fig. 2. Comparison between observed and SWAT model simulated streamflow at Bakel Station (1995–1999)

Table 3. Statistic Results for Calibration Period (1995–1998) and Validation Period (1999) of SWAT Model Streamflow Simulation at Bakel Station

Period	NSC	RMSE (m^3/s)	ME (m^3/s)
Calibration (1995–1998)	0.82	264.11	−72.44
Validation (1999)	0.82	528.40	−289.97

Error Quantification

The *true* state is a trade-off between model output and observation based on the comparison between their errors. Hence, the determination of the true state is essentially the quantification of the model errors and the observation errors. The model errors have various sources, such as inputs, parameters, model structure, boundary and initial conditions, and so forth (Liu and Gupta 2007). Underestimation or overestimation of the model error may cause the assimilation results to overly rely on the observations or the model output (Kitanidis and Bras 1980a). Observation errors are usually caused by the measurement method and/or equipment error. For example, streamflow observation errors are not only caused by the determination of the stage–discharge curve but may also be due to errors during the stage measurements.

In this paper, the model error covariance matrix **Q** is determined by the trial and error method, following Puente and Bras (1987). The observation error covariance matrix **R** is simply the stream flow variance. Assume the observation error is proportional to the scale of the streamflow observation (Clark et al. 2008), hence

$$R_k = (\alpha y_k)^2 \tag{18}$$

where y_k = observed stream flow; and $\alpha = 0.1$ = scaling factor determined by trial and error.

Despite the importance of error quantification, the trial and error method is still the mainstream method, and therefore, the error quantification process is often regarded as the *calibration* of the DA model. It is worth pointing out that observation errors and/or imperfect initialization of the model might be offset by cumulative update of the errors (Mehra 1972).

Output Assimilation

Output assimilation is based on the assumption that errors in the model output are additive. The sample autocorrelation functions (ACFs) of streamflow observation and the SWAT output errors show that although both have a strong autocorrelation for up to 20 days, the error ACF is less robust than the streamflow observation ACF. This indicates that the ARMA model with streamflow observation as extra input might produce better predictions.

For simplicity, 2 two-order AR models are suggested:

$$e(i+t) = a_1(i)e(i) + a_2(i)e(i-1) \tag{19}$$

$$e(i+t) = a_1(i)e(i) + a_2(i)e(i-1) + b_1(i)Q_{\text{obs}(i)} + b_2(i)Q\_\text{obs}(i-1) \tag{20}$$

where $e(i+t)$ = predicted error of t days ahead of day i; $a_1(i)$, $a_2(i)$, $b_1(i)$, $b_2(i)$ = time-variable coefficients calculated with the least linear square method; $e(i)$, $e(i-1)$ = errors of SWAT model output at day i and $i-1$; and $Q\_\text{obs}(i)$ and $Q\_\text{obs}(i-1)$ = streamflow observations at day i and day $i-1$, respectively.

With the predicted error, the predicted streamflow can be calculated with

$$Q(i+t) = Q_{ol}(i+t) + e(i+t) \tag{21}$$

where $Q_{ol}(i+t)$ = SWAT output of day $i+t$, assuming that the climate prediction is reliable.

Experimental Design

Four numerical experiments (Experiments A, B, C, and D) were designed to evaluate the performance of different assimilation schemes. Experiment A is an open-loop SWAT model without any assimilation. It is used as the reference experiment. Experiment B applies the AR models as output assimilation based on the output of Experiment A. Depending on the selection of AR inputs, Experiment B is further divided into two subexperiments: in experiment B-I, the inputs of the AR models are the errors between the model output and the observation for the previous two days [Eq. (19)]; In experiment B-II, the inputs are the errors as well as the observations of the previous two days [Eq. (20)]. The outputs of the two subexperiments are both calculated with Eq. (21). In Experiment C, EKF is used for state–parameter assimilation. EKF is first applied to SWAT continuously up to the date when the forecast is issued. Before that, SWAT is run in open-loop mode to issue forecasts Q_{ol}^{EKF}. In Experiment D, EKF and the AR model are used

simultaneously, but the error prediction model is not based on Experiment A, but rather Experiment C. This means that the model errors in both the training and validation stages refer to the differences between the observations and the outputs of the SWAT model for which the parameters have been updated using EKF. In forecasting mode, the errors are simply added to Q_{ol}^{EKF}. The AR model used to simulate the errors for 1992 (with respect to 1999) is trained with the 1990–1991 (with respect to 1990–1998) observations.

Three statistical performance indicators are used to assess the accuracy of the model prediction:

Root-mean-square error (m^3/s):

$$\mathrm{RMSE} = \sqrt{\frac{\sum_{i=1}^{N}(Q_i^o - Q_i^s)^2}{N}} \tag{22}$$

Nash–Sutcliffe coefficient:

$$\mathrm{NSC} = 1 - \frac{\sum_{i=1}^{N}(Q_i^o - Q_i^s)^2}{\sum_{i=1}^{N}(Q_i^o - \overline{Q^o})^2} \tag{23}$$

Mean error:

$$\mathrm{ME} = \frac{\sum_{i=1}^{N}(Q_i^s - Q_i^o)}{N} \tag{24}$$

where N = time series length (in days); Q_i^o (m^3/s) = streamflow observation of the ith day; $\overline{Q^o}$ (m^3/s) = mean of the true streamflow series; and Q_i^s (m^3/s) = model's prediction of the ith day.

Results and Analysis

State–Parameter Assimilation

Assimilation Results

The comparisons between the EKF assimilation and the open-loop model output at Bakel Station for 1992 and 1999 are shown in Figs. 3(a and b). For 1992, SWAT in open-loop mode (Experiment A, thin line) mostly overestimates the observed streamflow (thick line). For 1999, SWAT in open-loop mode overestimates the dry season streamflow but significantly underestimates the wet season flood. The EKF assimilated streamflow (dashed line) is similar in the observations versus the model output for both years. This indicates that there is a higher confidence in the observation than in the model output.

The grey dashed line represents the values of Kalman gain K for the streamflow. With high K values, the model output is not considered by the EKF assimilation for the dry season. K drops to lower values only in major flood periods. One of the possible reasons for this is that the majority of the streamflow in the dry season is base flow originating from ground water, although the state vector only contains water storage variables and parameters that are critical to surface and lateral runoff. In addition, given that the model errors are set to be constant whereas the observation errors are proportional to the scale of the streamflow, the larger observation errors give the model outputs more confidence, leading to lower K values. Considering the distinctively different performances of EKF before and after July 1, the streamflow forecasts

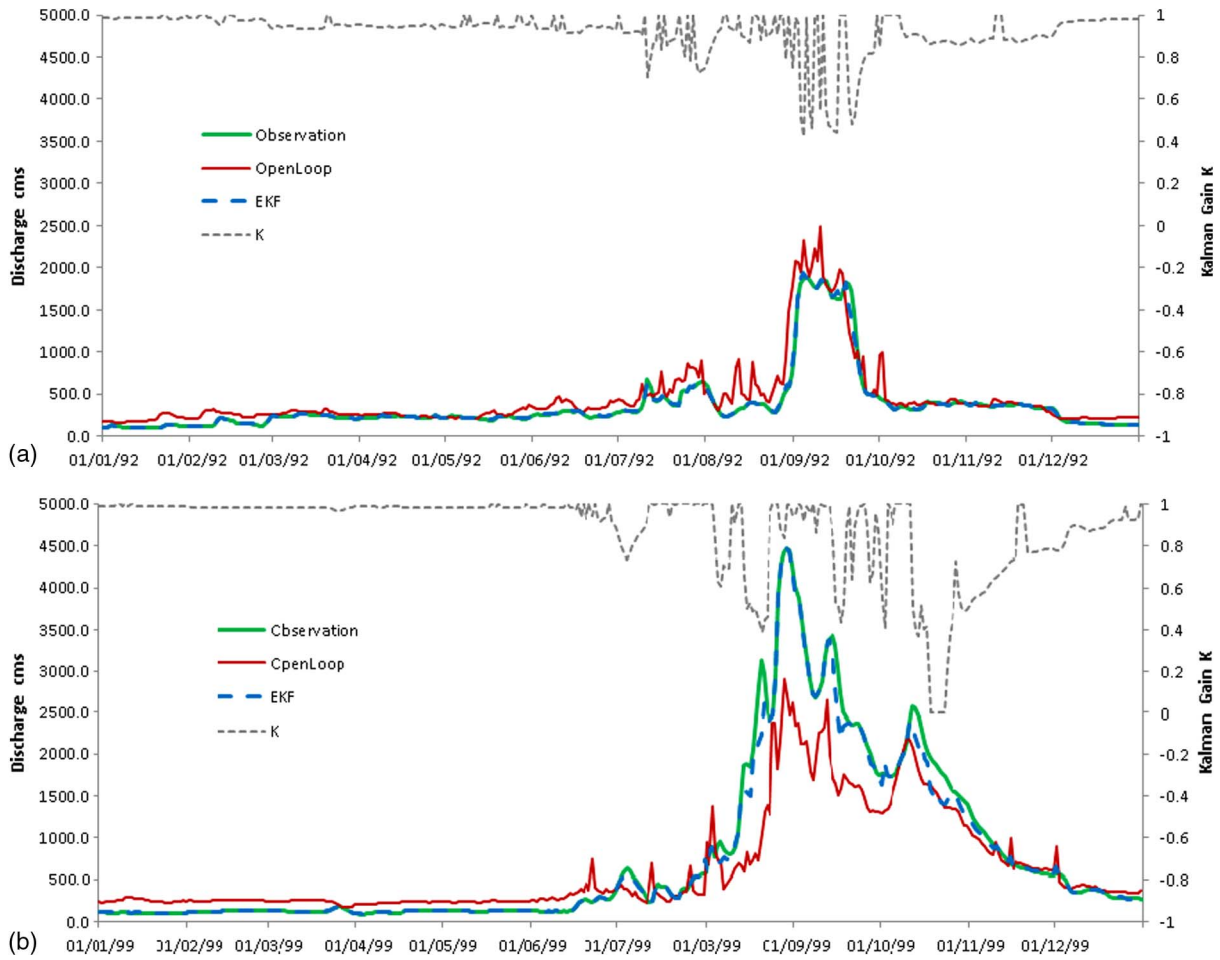

Fig. 3. Streamflow EKF assimilation results compared to observation and open-loop: (a): 1992; (b) 1999

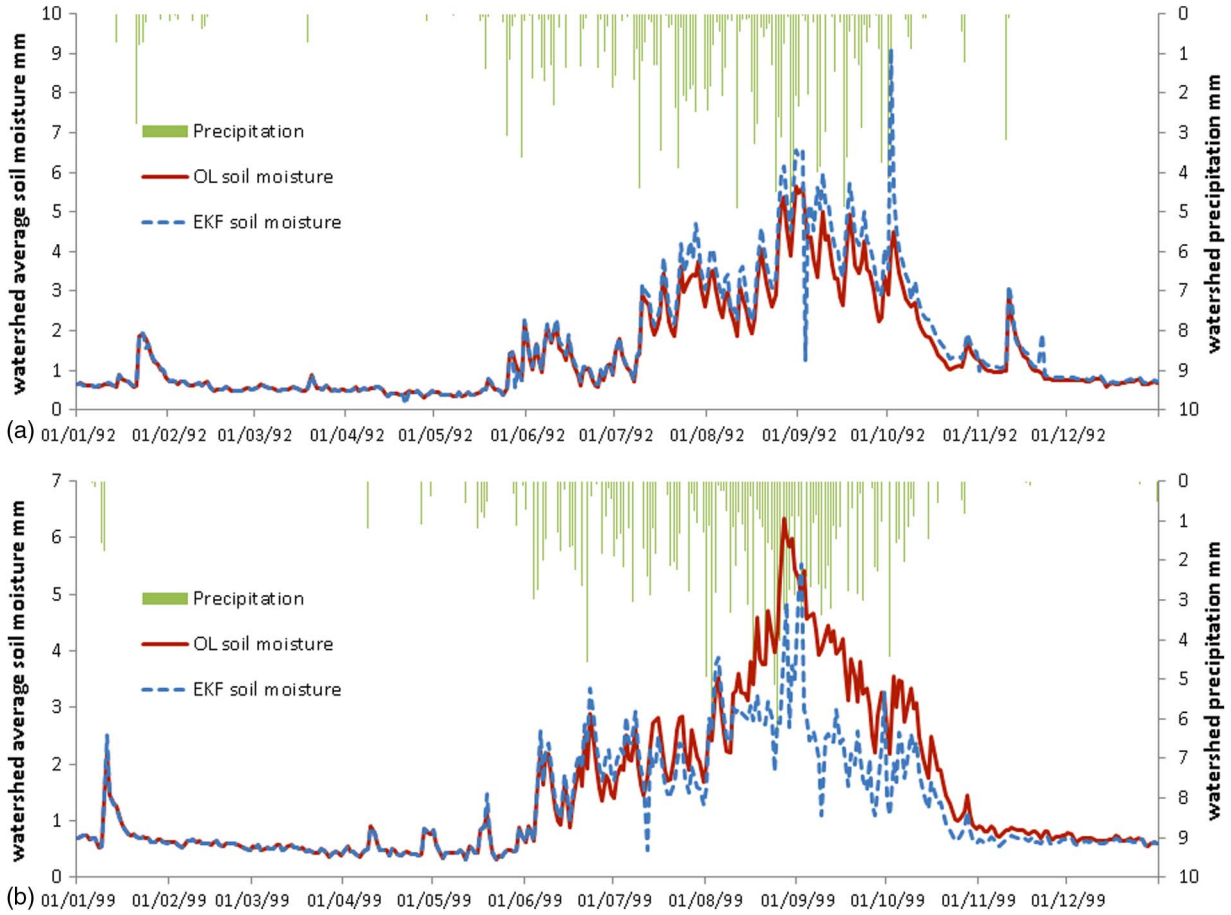

Fig. 4. Watershed average soil moisture (millimeter) EKF assimilation results compared to open-loop (OL): (a) 1992; (b) 1999

from July to December are discussed separately as *wet season* streamflow in the following sections (unless the term *wet season* is specifically redefined).

The soil moisture assimilation results for 1992 and 1999 at the watershed scale are shown in Figs. 4(a and b) respectively. In both years, the soil moisture increases significantly in the wet season. Despite some fluctuations, applying EKF increases the soil moisture estimation for the wet season of 1992. In contrast, applying EKF significantly reduces the soil moisture estimation for the wet season of 1999, especially during the flood peak period. Notice that the SWAT model overestimates the flood in 1992 whereas it underestimates the flood in 1999.

Because of the scarcity of in situ watershed soil moisture measurements, it is challenging to verify the soil moisture assimilation results of EKF. The different update patterns for 1992 and 1999 reveal that EKF assimilation is influenced more by the accumulation of precipitation than the intensity of a single precipitation event. Compared to streamflow, the soil moisture is more sensitive to watershed precipitation. This implies that the simulation results of specific soil moisture models that use precipitation as input may provide more accurate soil moisture state estimates (Hopmans et al. 2002; Montzka et al. 2013).

Fig. 5 displays the updates for CN2 and dailyCN through 1990–1999. DailyCN is the soil moisture adjusted curve number used in

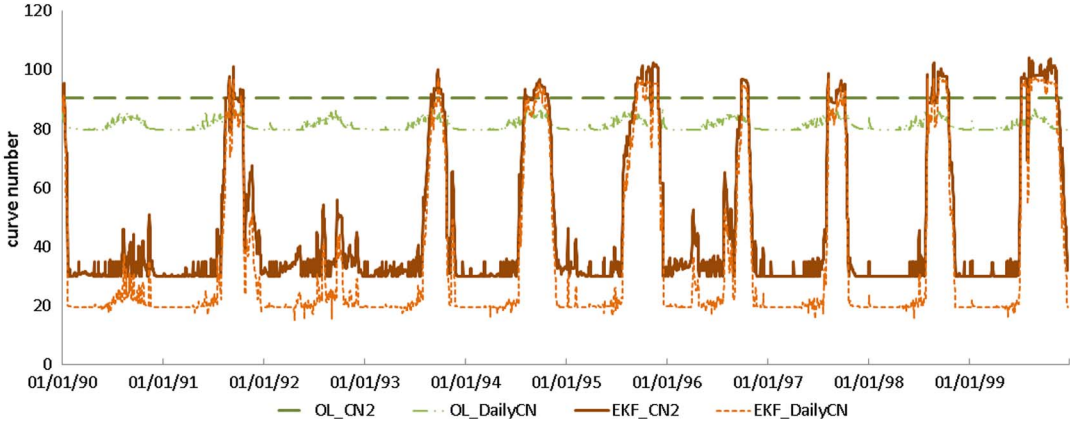

Fig. 5. Update of CN2 and dailyCN with EKF assimilation through 1990–1999

the final surface runoff calculation [Eqs. (14)–(16)]. Both CN2 and dailyCN are directly proportional to the surface runoff generation (i.e., a larger curve number leads to larger runoff, and subsequently, increased streamflow). In SWAT, CN2 remains constant unless it is redefined in future crop operation processes, whereas dailyCN varies with the soil moisture content. The traditional batch calibration technologies assume that the calibrated model is robust enough (at least for the validation period). However, as shown in Fig. 2, the calibrated model does not perform well for the exceptional flood in 1999.

The EKF updated curve number shows dramatically different patterns from those in the open-loop case. Both CN2 and dailyCN are greatly reduced in the dry season, whereas they are significantly increased in the flood season. CN2 and dailyCN are reduced during the flood period of 1992; however, they are increased during the flood period of 1999. Both correctly reflect the streamflow update results in Figs. 3(a and b). DailyCN sees more fluctuations than CN2 because soil moisture is also adjusted by EKF. It is interesting to observe that, despite the curve numbers not actually being used in the dry season because of the absence of surface runoff, EKF still tries to *drag down* the curve numbers in order to reduce the streamflow overestimation of the SWAT open-loop simulation.

Streamflow Forecast Improvement

In order to verify the improvement in SWAT streamflow forecasts due to the state–parameter assimilation with EKF, the one- to seven-day SWAT streamflow forecasts after using EKF are evaluated. A full hydrograph is obtained for each lead because EKF is applied continuously. To avoid confusion, the open-loop forecasts issued after the application of EKF up to the date the forecast is issued are termed EKF subsequent open-loop (EKFsOL). Figs. 6(a and b) show the hydrographs of these EKFsOL results for 1992 and 1999, respectively.

The EKFsOL provides better results than the SWAT open-loop (OL) simulation (without using EKF) in both years. As shown in Figs. 6(a and b), the streamflow fluctuations observed when OL is used are mostly eliminated, and the flood is less overestimated when EKFsOL is used. The statistic indicators of Experiment C are summarized in Tables 4 and 5. The NSC for the one-day forecast in wet seasons is improved to 0.91 from 0.77 in open-loop simulation, the RMSE is reduced to 138.60 from 223.08 m^3/s, and ME is reduced to 40.96 from 100.48 m^3/s. In 1999, the NSC is improved to 0.88 from 0.63, the RMSE is reduced to 207.41 from 670.45 m^3/s, and the ME is reduced to −41.25 from −365.83 m^3/s.

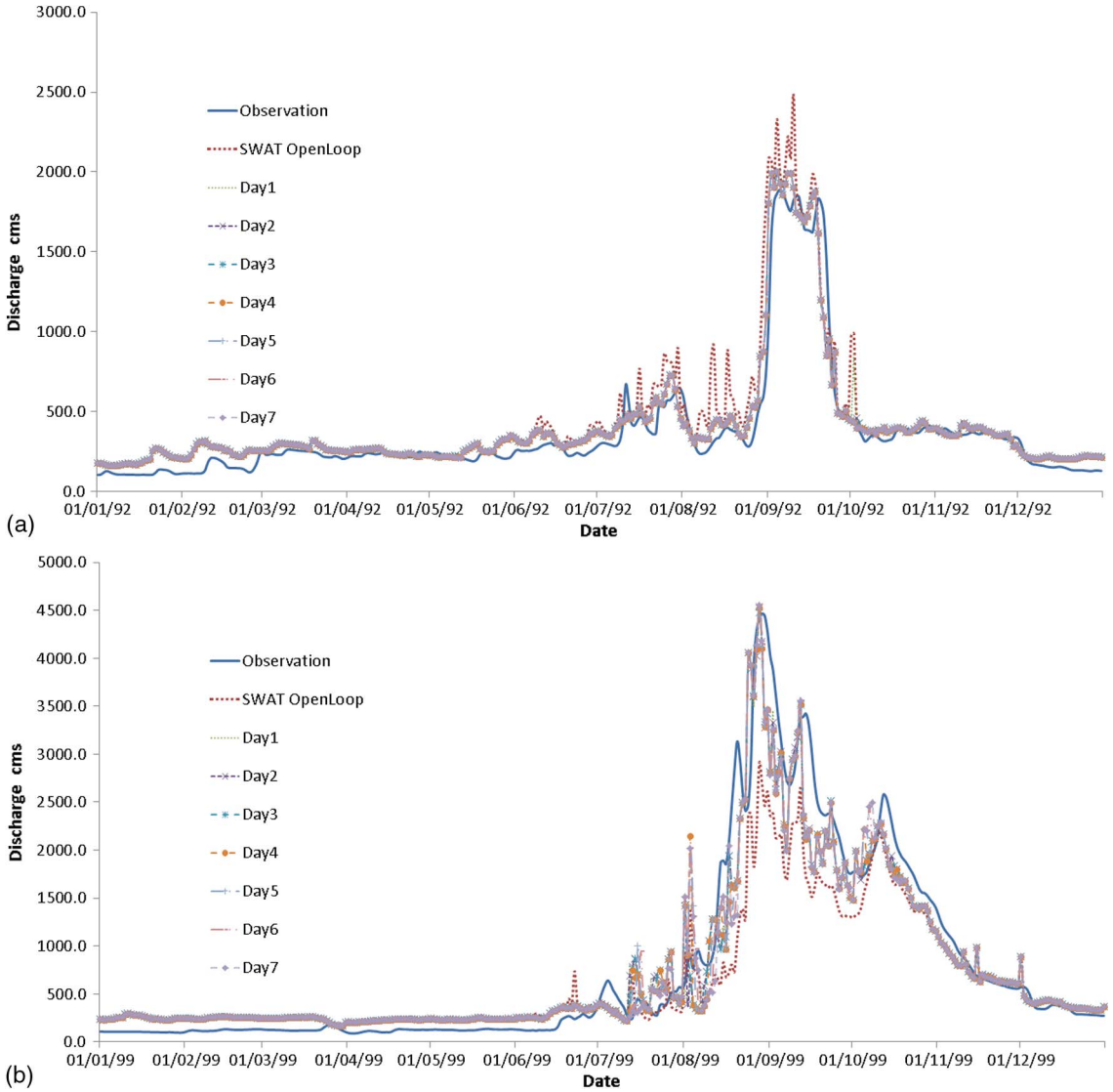

Fig. 6. EKF subsequent open-loop (EKFsOL) streamflow forecast: (a) 1992; (b) 1999

J. Hydrol. Eng., 2017, 22(3): 04016060

Table 4. One- to Seven-Day Forecast Results for Three Assimilation Experiments in Wet Season of 1992

1992 wet season	Experiment B-II			Experiment C			Experiment D		
	RMSE (m^3/s)	NSC	ME (m^3/s)	RMSE (m^3/s)	NSC	ME (m^3/s)	RMSE (m^3/s)	NSC	ME (m^3/s)
Experiment A	223.08	0.77	100.48	223.08	0.77	100.48	223.08	0.77	100.48
Day 1	141.85	0.91	11.02	138.60	0.91	40.96	95.32	0.96	0.88
Day 2	191.71	0.83	11.95	134.87	0.92	38.63	127.62	0.93	−1.20
Day 3	205.04	0.81	11.95	134.83	0.92	38.34	143.10	0.91	−4.10
Day 4	206.85	0.80	12.28	134.83	0.92	38.24	148.54	0.90	−5.96
Day 5	205.00	0.81	13.57	134.88	0.92	38.21	146.91	0.90	−7.21
Day 6	203.84	0.81	15.83	134.93	0.92	38.19	144.15	0.90	−7.29
Day 7	204.68	0.81	16.18	134.96	0.92	38.23	144.83	0.90	−7.28
Average	194.14	0.82	13.25	135.41	0.92	38.69	135.78	0.91	−4.60

Note: Experiment B-II = AR model; Experiment C = EKF model; Experiment D = hybrid model.

Table 5. One- to Seven-Day Forecast Results for Three Assimilation Experiments in Wet Season of 1999

1999 wet season	Experiment B-II			Experiment C			Experiment D		
	RMSE (m^3/s)	NSC	ME (m^3/s)	RMSE (m^3/s)	NSC	ME (m^3/s)	RMSE (m^3/s)	NSC	ME (m^3/s)
Experiment A	670.46	0.63	−375.83	670.45	0.63	−375.83	670.45	0.63	−375.83
Day 1	400.94	0.87	−134.74	207.41	0.96	−41.52	266.02	0.94	−36.91
Day 2	412.60	0.86	−132.24	290.48	0.93	−86.73	337.36	0.91	−77.30
Day 3	413.83	0.86	−133.53	350.16	0.90	−127.10	376.20	0.88	−119.19
Day 4	425.08	0.85	−129.14	406.61	0.86	−154.44	407.60	0.86	−143.40
Day 5	428.37	0.85	−128.86	428.20	0.85	−162.03	414.86	0.86	−147.58
Day 6	429.98	0.85	−130.33	443.15	0.84	−168.61	420.60	0.85	−151.07
Day 7	432.15	0.85	−132.90	447.22	0.83	−163.33	427.14	0.85	−147.58
Average	420.42	0.85	−131.68	367.60	0.88	−129.11	378.54	0.88	−117.58

Note: Experiment B-II = AR model; Experiment C = EKF model; Experiment D = hybrid model.

Output Assimilation Results

The single-variable input experiment B-I only uses the errors from the previous two days, whereas the multivariable input experiment B-II also uses streamflow observations. The accuracy of both subexperiments decreases rapidly for the first four days as the lead gets longer. No obvious differences between these two subexperiments were observed for 1992, whereas B-II significantly outperforms B-I for 1999. The better performance of the combined input experiments agrees with the results from other research (Anctil et al. 2003; Jeevaragagam and Simonovic 2013).

Figs. 7(a and b) show the forecasts of subexperiment B-II, whose RMSE, NSC, and ME values for the wet seasons of 1992 and 1999 are presented in Tables 4 and 5. A major difference between subexperiment B-II and Experiment C is that the former predicts the streamflow of the dry season better than the wet season, whereas the latter does not improve dry season prediction. The dry season streamflow is more stable, which is easier for the AR model to handle. EKF only updates the states and parameters related to surface and lateral runoff, which in the dry season contributes little to the channel streamflow.

For 1992, the AR model provides accurate results for one-day forecasts, but accuracy decreases rapidly for the two-day and longer forecasts. As shown in Fig. 7(a), the forecasts for longer leads have more fluctuations than the values from the observations. More importantly, the flood peak is often underestimated. The 1999 forecasts are generally very accurate compared to SWAT open-loop simulations with more robustness than 1992.

Experiment D is designed to combine EKF with the AR model: instead of assimilating the errors between the SWAT open-loop simulation and the observations, as Experiment B does, the errors between the EKFsOL and the observation are assimilated into the model outputs. The idea behind this experiment is that the filtered model errors might be more suitable for the AR model. Note that the EKFsOL have seven time series, but only the one-day forecast series is used in Experiment D because it is the most accurate forecast among the seven.

The forecasts of Experiment D for 1992 and 1999 are shown in Figs. 8(a and b), respectively, and their RMSE and NSC results are presented in Tables 4 and 5. In 1992, Experiment D significantly outperforms Experiment B for all leads. The NSC, RMSE, and ME of the one-day wet season forecast for Experiment B-II are 0.91, 141.85, and 11.02 m^3/s, but 0.96, 95.32, and 0.88 m^3/s for Experiment D. NSC, RMSE, and ME of the seven-day wet season forecast for Experiment B-II are 0.81, 204.68, and 16.18 m^3/s, but 0.90, 144.83, and −7.28 m^3/s for Experiment D. The forecasts for different leads are more clustered, indicating more stability and less sensitivity to lead length. In 1999, notable improvement compared to Experiment B can only be found for leads shorter than four days. Comparing Figs. 7(b) and 8(b), it is also found that Experiment D produces *smoother* forecasts than Experiment B. Furthermore, Experiment D provides more accurate forecasts for the flood rising limb and flood peak discharge from early August to early September, whereas Experiment B captures more features of the flood recession period after mid-September. These are valuable findings if these methods are to be applied in an operational flood forecasting and warning system.

Comparison of Experiments

The comparison of the wet season forecasts of all the experiments is shown in Tables 4 and 5. Because the EKF assimilation is not effective in the dry season, only wet season results are calculated here.

All three assimilation experiments significantly improve upon Experiment A (the open-loop SWAT simulation without any assimilation). In 1992, the average RMSE for all seven-day forecasts of Experiment B, C, and D are 194.14, 135.41, and 135.78 m^3/s

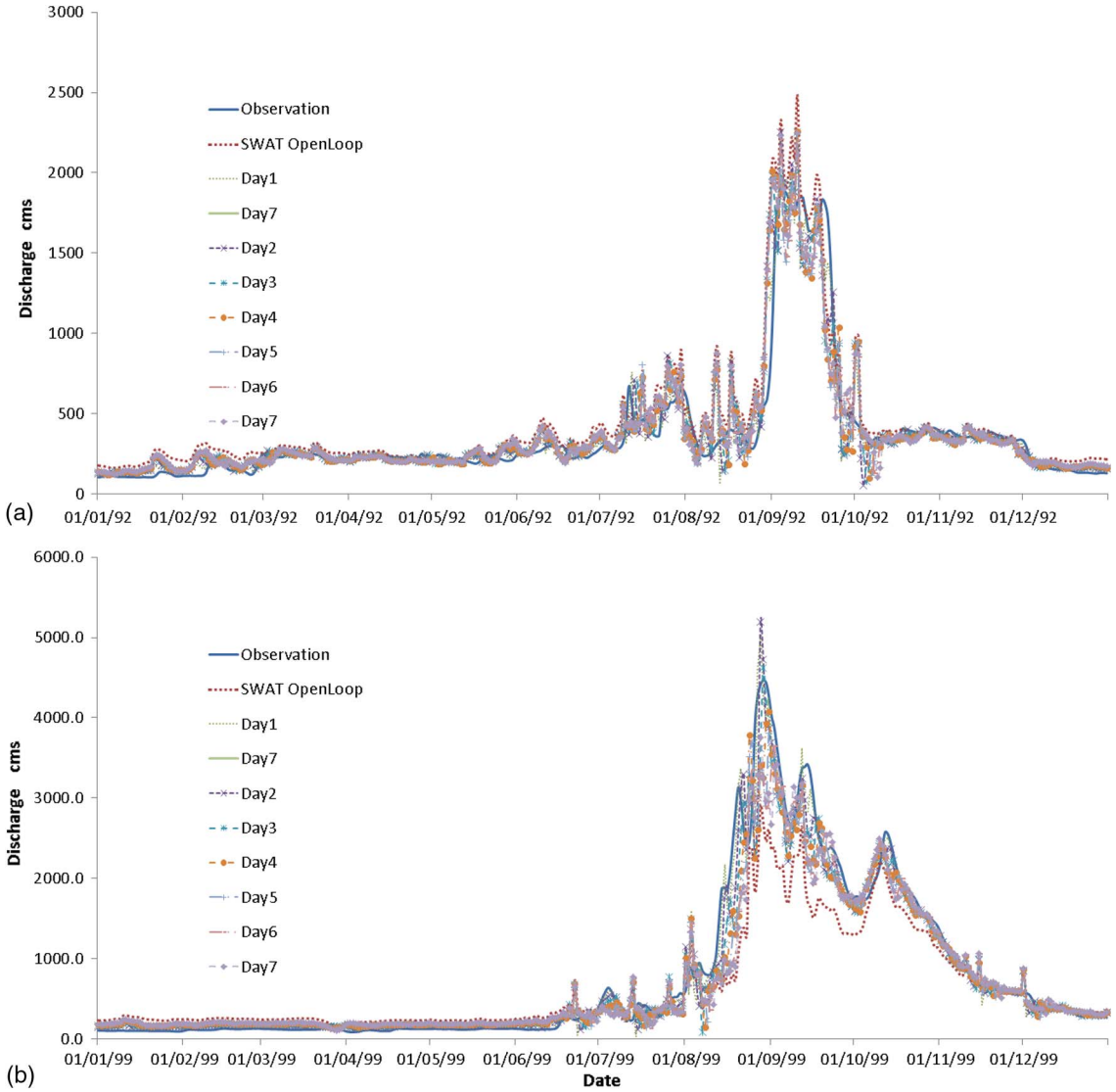

Fig. 7. Streamflow forecasts for different lead days of the multivariable input AR model (Experiment B-II): (a) 1992, full year; (b) 1999, full year

versus the 223.08 m^3/s of Experiment A. The average ME of Experiment B, C, and D are 13.25, 38.69, and -4.60 m^3/s versus the 100.48 m^3/s of Experiment A. In 1999, the average RMSE of Experiment A is 670.46 m^3/s, but 420.42, 367.60, and 378.54 m^3/s for B, C, and D, respectively. The average ME of Experiment A is -375.83 m^3/s, but -131.68, -129.11, and -117.58 m^3/s for B, C, and D, respectively.

In 1992, the improvement with Experiment C is less sensitive to the increase of leads compared to other experiments, whereas in 1999 it is Experiment B that is less sensitive. It is noticed that the state–parameter assimilation (Experiment C) outperforms output assimilation (Experiment B) for the dry year 1992 measured by RMSE and NSC (although the latter has better ME). However, output assimilation slightly outperforms state–parameter assimilation for longer forecasts in the wet year of 1999. For example, in 1999 the seven-day forecast NSC, RMSE, and ME for output assimilation are 0.85, 432.15 m^3/s, and -132.90 m^3/s, versus 0.83, 447.22 m^3/s, and -163.33 m^3/s for state–parameter assimilation. The benefit of state–parameter assimilation on streamflow forecast depends on the effectiveness of the updated initial condition. For longer forecasts in a wet year, the frequent occurrence of precipitation during the forecast period likely offsets the benefit of an updated initial condition.

The hybrid assimilation (Experiment D) provides more accurate forecast results in both dry and wet years. As mentioned before, although state–parameter assimilation usually outperforms output assimilation on RMSE and NSC, the latter has better ME. The combined assimilation balances the two with RMSE and NSC better than output assimilation, and ME better than state–parameter assimilation.

Conclusions

This paper discussed the application of two widely used hydrological data assimilation methods (state–parameter assimilation and output assimilation) in streamflow forecast scenarios. Based on a SWAT model, EKF is used as the state–parameter assimilation, and AR models are used as the output assimilation.

It is found that although both methods could improve the forecast accuracy, their performance is influenced by the hydrological regime of the year. For shorter forecast leads, the state–parameter assimilation outperforms the output assimilation in both dry and wet years. For longer forecast leads, the output assimilation could provide slightly superior results in the wet years. The flood rising limb and peak discharge are more accurately forecast by the

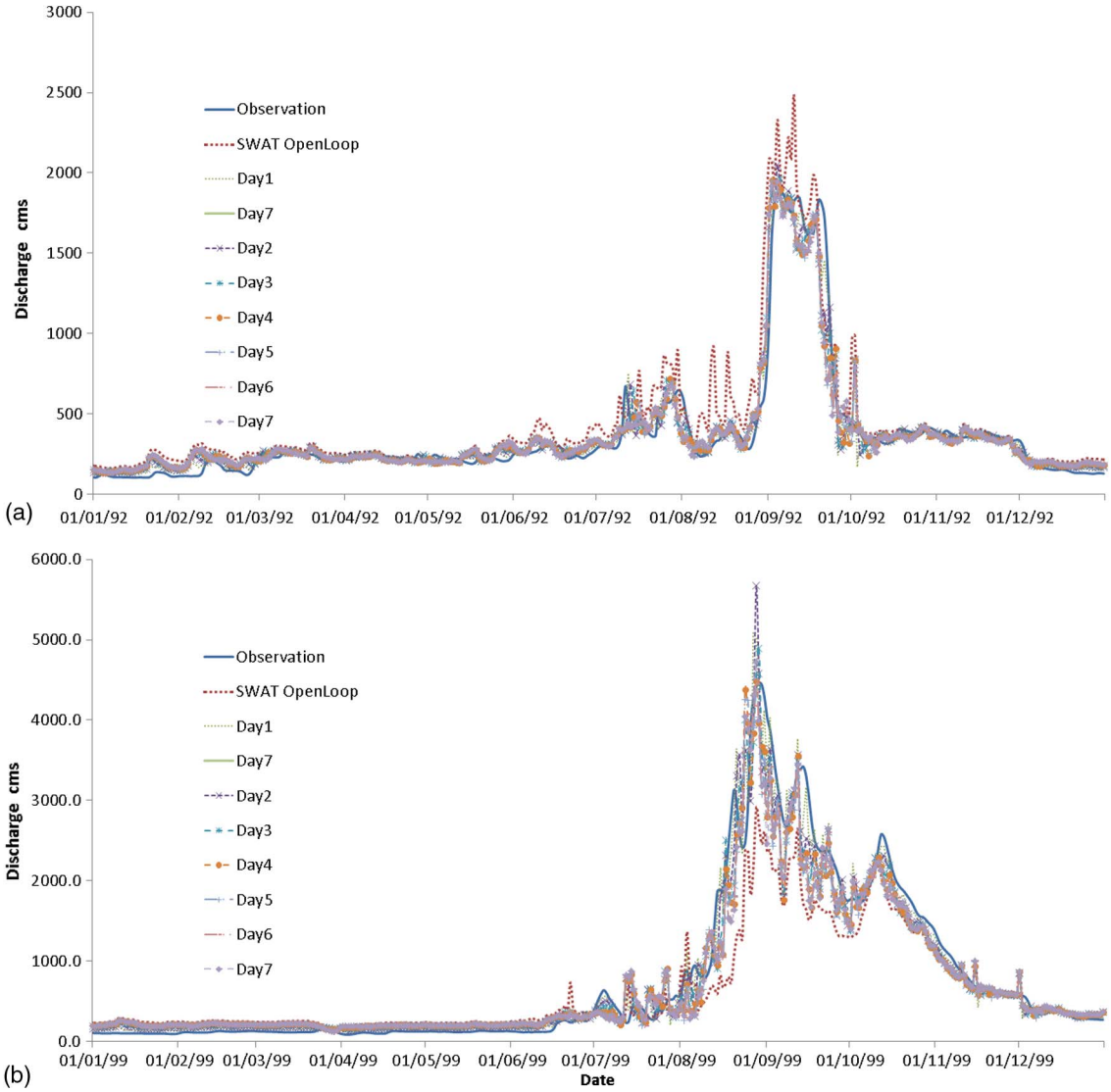

Fig. 8. Streamflow forecasts for different lead days of the hybrid model (Experiment D): (a) 1992, full year; (b) 1999, full year

state–parameter assimilation, whereas the recession limb is better captured by the output assimilation.

The traditional state and output hybrid methods only focus on the hydrodynamic module of a hydrological model. In this study, we coupled output assimilation with state–parameter assimilation that works on the rainfall-runoff part of SWAT. The new hybrid method combines the advantage of the two methods with overall outstanding performance in both dry and wet years measured by all three indicators: RMSE, NSC, and ME.

In conclusion, it is found that, in general, state–parameter assimilation is superior to output assimilation. However, the hybrid method seems to be very promising with its robustness and flexibility in different hydrological regimes and forecasting lengths. The methodology and founding of this study have great potential in operational flood forecasting (assuming that the weather input is reliable) given the simplicity and limited computational cost it involves.

Acknowledgments

The authors thank Robert Hart for his proofreading of this paper. The data used in this study are available upon request to the corresponding author.

References

Ajami, N. K., Duan, Q., and Sorooshian, S. (2007). "An integrated hydrologic Bayesian multimodel combination framework: Confronting input, parameter, and model structural uncertainty in hydrologic prediction." *Water Resour. Res.*, 43(1), W01403.

Anctil, F., Perrin, C., and Andréassian, V. (2003). "ANN output updating of lumped conceptual rainfall/runoff forecasting models." *J. Am. Water Resour. Assoc.*, 39(5), 1269–1279.

Anctil, F., Perrin, C., and Andréassian, V. (2004). "Impact of the length of observed records on the performance of ANN and of conceptual parsimonious rainfall-runoff forecasting models." *Environ. Modell. Software*, 19(4), 357–368.

Angela, L. (1982). "Combination of a conceptual model and an autoregressive error model for improving short time forecasting." *Hydrol. Res.*, 13(4), 233–246.

Arnold, J. G., Srinivasan, R., Muttiah, S. R., and Williams, J. R. (1998). "Large area hydrologic modeling and assessment. I: Model development." *J. Am. Water Resour. Assoc.*, 34(1), 73–89.

Bauer-Gottwein, P., Jensen, I., Guzinski, R., Bredtoft, G., Hansen, S., and Michailovsky, C. (2015). "Operational river discharge forecasting in poorly gauged basins: The Kavango River Basin case study." *Hydrol. Earth Syst. Sci.*, 19(3), 1469–1485.

Berg, A. A., and Mulroy, K. A. (2006). "Streamflow predictability in the Saskatchewan/Nelson River Basin given macroscale

estimates of the initial soil moisture status." *Hydrol. Sci. J.*, 51(4), 642–654.
Berger, K. P., and Entekhabi, D. (2001). "Basin hydrologic response relations to distributed physiographic descriptors and climate." *J. Hydrol.*, 247(3), 169–182.
Berthet, L., Andréassian, V., Perrin, C., and Javelle, P. (2009). "How crucial is it to account for the antecedent moisture conditions in flood forecasting? Comparison of event-based and continuous approaches on 178 catchments." *Hydrol. Earth Syst. Sci. Discuss.*, 13(6), 819–831.
Beven, K. (1989). "Changing ideas in hydrology—The case of physically-based models." *J. Hydrol.*, 105(1), 157–172.
Bidwell, V., and Griffiths, G. (1994). "Adaptive flood forecasting: An application to the Waimakariri River." *J. Hydrol.*, 32(2), 1–15.
Box, G. E., and Jenkins, G. M. (1976). "Time series analysis: Forecasting and control." *Holden-Day series in time series analysis*, Holden-Day, San Francisco.
Brocca, L., Melone, F., Moramarco, T., and Singh, V. (2009). "Assimilation of observed soil moisture data in storm rainfall-runoff modeling." *J. Hydrol. Eng.*, 10.1061/(ASCE)1084-0699(2009)14:2(153), 153–165.
Broersen, P. M. (2007). "Error correction of rainfall-runoff models with the ARMAsel program." *IEEE Trans. Instrum. Meas.*, 56(6), 2212–2219.
Broersen, P. M., and Weerts, A. H. (2005). "Automatic error correction of rainfall-runoff models in flood forecasting systems." *Proc., IEEE Instrumentation and Measurement Technology Conf., 2005. IMTC 2005*, IEEE, New York.
Chen, F., Crow, T. W., and Ryu, D. (2014). "Dual forcing and state correction via soil moisture assimilation for improved rainfall-runoff modeling." *J. Hydrometeorol.*, 15(5), 1832–1848.
Chen, L., Zhang, Y., Zhou, J., Singh, P. V., Guo, S., and Zhang, J. (2015). "Real-time error correction method combined with combination flood forecasting technique for improving the accuracy of flood forecasting." *J. Hydrol.*, 521(Feb), 157–169.
Choi, B. (2012). *ARMA model identification*, Springer, New York.
Clark, M. P., et al. (2008). "Hydrological data assimilation with the ensemble Kalman filter: Use of streamflow observations to update states in a distributed hydrological model." *Adv. Water Resour.*, 31(10), 1309–1324.
Cloke, H., and Pappenberger, F. (2009). "Ensemble flood forecasting: A review." *J. Hydrol.*, 375(3), 613–626.
De Kleermaeker, S., and Verkade, J. (2013). "A decision support system for use of probability forecasts." *ISCRAM 2013: Proc., 10th Int. Conf. on Information Systems for Crisis Response and Management*, ISCRAM Association, KIT, Karlsruhe, Germany.
Evensen, G. (1994). "Sequential data assimilation with a nonlinear quasi-geostrophic model using Monte Carlo methods to forecast error statistics." *J. Geophys. Res.*, 99(C5), 10143–10162.
Garen, D. C. (1992). "Improved techniques in regression-based streamflow volume forecasting." *J. Water Resour. Plann. Manage.*, 10.1061/(ASCE)0733-9496(1992)118:6(654), 654–670.
Georgakakos, K. P., Seo, D.-J., Gupta, H., Schaake, J., and Butts, M. B. (2004). "Towards the characterization of streamflow simulation uncertainty through multimodel ensembles." *J. Hydrol.*, 298(1), 222–241.
Hendricks Franssen, H., and Kinzelbach, W. (2008). "Real-time groundwater flow modeling with the ensemble Kalman filter: Joint estimation of states and parameters and the filter inbreeding problem." *Water Resour. Res.*, 44(9), W09408.
Hopmans, J. W., Nielsen, R. D., and Bristow, K. L. (2002). "How useful are small-scale soil hydraulic property measurements for large-scale vadose zone modeling?" *Heat and mass transfer in the natural environment, the philip volume*. D. Smiles, P. A. C. Raats, and A. Warrick, eds., *Geophysical Monograph Series*, American Geophysical Union, Washington, DC, 129, 247–258.
Jacobs, J. M., Myers, A. D., and Whitfield, B. M. (2003). "Improved rainfall/runoff estimates using remotely sensed soil moisture." *J. Am. Water Resour. Assoc.*, 39(2), 313–324.
Jain, A., and Srinivasulu, S. (2004). "Development of effective and efficient rainfall-runoff models using integration of deterministic, real-coded genetic algorithms and artificial neural network techniques." *Water Resour. Res.*, 40(4), W04302.
Javelle, P., Fouchier, C., Arnaud, P., and Lavabre, J. (2010). "Flash flood warning at ungauged locations using radar rainfall and antecedent soil moisture estimations." *J. Hydrol.*, 394(1–2), 267–274.
Jayakrishnan, R., Srinivasan, R., Santhi, C., and Arnold, J. G. (2005). "Advances in the application of the SWAT model for water resources management." *Hydrol. Processes*, 19(3), 749–762.
Jeevaragagam, P., and Simonovic, S. P. (2013). "Improvement of streamflow simulation for gauged site of hydrological model." *Malaysian J. Civ. Eng.*, 25(2), 239–253.
Jeong, D. I., and Kim, Y.-O. (2009). "Combining single-value streamflow forecasts—A review and guidelines for selecting techniques." *J. Hydrol.*, 377(3), 284–299.
Kalman, R. E. (1960). "A new approach to linear filtering and prediction problems." *Trans. ASME–J. Basic Eng.*, 82(Series D), 35–45.
Khac-Tien Nguyen, P., and Hock-Chye Chua, L. (2012). "The data-driven approach as an operational real-time flood forecasting model." *Hydrol. Processes*, 26(19), 2878–2893.
Kitanidis, P. K., and Bras, R. L. (1980a). "Real-time forecasting with a conceptual hydrologic model. I: Analysis of uncertainty." *Water Resour. Res.*, 16(6), 1025–1033.
Kitanidis, P. K., and Bras, R. L. (1980b). "Real-time forecasting with a conceptual hydrologic model. II: Applications and results." *Water Resour. Res.*, 16(6), 1034–1044.
Krzysztofowicz, R. (1999). "Bayesian theory of probabilistic forecasting via deterministic hydrologic model." *Water Resour. Res.*, 35(9), 2739–2750.
Krzysztofowicz, R. (2001). "The case for probabilistic forecasting in hydrology." *J. Hydrol.*, 249(1), 2–9.
Liu, Y., and Gupta, H. V. (2007). "Uncertainty in hydrologic modeling: Toward an integrated data assimilation framework." *Water Resour. Res.*, 43(7), W07401.
Lü, H., et al. (2010). "Using a H∞ filter assimilation procedure to estimate root zone soil water content." *Hydrol. Processes*, 24(25), 3648–3660.
Lü, H., Yu, Z., Zhu, Y., Drake, S., Hao, Z., and Sudicky, E. A. (2011). "Dual state-parameter estimation of root zone soil moisture by optimal parameter estimation and extended Kalman filter data assimilation." *Adv. Water Resour.*, 34(3), 395–406.
Madsen, H., and Skotner, C. (2005). "Adaptive state updating in real-time river flow forecasting—A combined filtering and error forecasting procedure." *J. Hydrol.*, 308(1), 302–312.
Massari, C., Brocca, L., Moramarco, T., Tramblay, Y., and Lescot, J.-F. D. (2014). "Potential of soil moisture observations in flood modelling: Estimating initial conditions and correcting rainfall." *Adv. Water Resour.*, 74(Dec), 44–53.
McMillan, H., Hreinsson, E., Clark, M., Singh, S., Zammit, C., and Uddstrom, M. (2013). "Operational hydrological data assimilation with the recursive ensemble Kalman filter." *Hydrol. Earth Syst. Sci.*, 17(1), 21–38.
Mehra, R. K. (1972). "Approaches to adaptive filtering." *IEEE Trans. Autom. Control*, 17(5), 693–698.
Montzka, C., et al. (2013). "Estimation of radiative transfer parameters from L-band passive microwave brightness temperatures using advanced data assimilation." *Vadose Zone J.*, 12(3), in press.
Moradkhani, H. (2008). "Hydrologic remote sensing and land surface data assimilation." *Sensors*, 8(5), 2986–3004.
Moradkhani, H., Hsu, L. K., Gupta, H., and Sorooshian, S. (2005a). "Uncertainty assessment of hydrologic model states and parameters: Sequential data assimilation using the particle filter." *Water Resour. Res. Water Resour. Res.*, 41(5), W05012.
Moradkhani, H., Sorooshian, S., Gupta, V. H., and Houser, P. R. (2005b). "Dual state-parameter estimation of hydrological models using ensemble Kalman filter." *Adv. Water Resour.*, 28(2), 135–147.
Muluye, G. Y. (2011). "Improving long-range hydrological forecasts with extended Kalman filters." *Hydrol. Sci. J.*, 56(7), 1118–1128.
Pagano, T., Wang, Q., Hapuarachchi, P., and Robertson, D. (2011). "A dual-pass error-correction technique for forecasting streamflow." *J. Hydrol.*, 405(3), 367–381.
Pham, D. T. (2001). "Stochastic methods for sequential data assimilation in strongly nonlinear systems." *Monthly Weather Rev.*, 129(5), 1194–1207.

Puente, C. E., and Bras, R. L. (1987). "Application of nonlinear filtering in the real-time forecasting of river flows." *Water Resour. Res.*, 23(4), 675–682.
Samuel, J., Coulibaly, P., Dumedah, G., and Moradkhani, H. (2014). "Assessing model state and forecasts variation in hydrologic data assimilation." *J. Hydrol.*, 513(May), 127–141.
Sene, K. (2008). *Flood warning, forecasting and emergency response*, Springer, Berlin.
Srinivasan, R., Ramanarayanan, S. T., Arnold, G. J., and Bednarz, S. T. (1998). "Large area hydrologic modeling and assessment. II: Model application." *J. Am. Water Resour. Assoc.*, 34(1), 91–101.
Ssegane, H., Tollner, E., Mohamoud, Y., Rasmussen, T., and Dowd, J. (2012). "Advances in variable selection methods. I: Causal selection methods versus stepwise regression and principal component analysis on data of known and unknown functional relationships." *J. Hydrol.*, 438–439(May), 16–25.
Sun, L., Nistor, I., and Seidou, O. (2015). "Streamflow data assimilation in SWAT model using extended Kalman filter." *J. Hydrol.*, 531(Dec), 671–684.
Tingsanchali, T., and Gautam, M. R. (2000). "Application of tank, NAM, ARMA and neural network models to flood forecasting." *Hydrol. Processes*, 14(14), 2473–2487.
Todini, E. (1988). "Rainfall-runoff modeling—Past, present and future." *J. Hydrol.*, 100(1), 341–352.
Todini, E. (2007). "Hydrological catchment modelling: Past, present and future." *Hydrol. Earth Syst. Sci.*, 11(1), 468–482.
Velázquez, J., Anctil, F., Ramos, M., and Perrin, C. (2011). "Can a multi-model approach improve hydrological ensemble forecasting? A study on 29 French catchments using 16 hydrological model structures." *Adv. Geosci.*, 29(Feb), 33–42.
Vrugt, J. A., Diks, G. C., Gupta, V. H., Bouten, W., and Verstraten, J. M. (2005). "Improved treatment of uncertainty in hydrologic modeling: Combining the strengths of global optimization and data assimilation." *Water Resour. Res.*, 41(1), W01017.
Vrugt, J. A., Gupta, V. H., Nualláin, B., and Bouten, W. (2006). "Real-time data assimilation for operational ensemble streamflow forecasting." *J. Hydrometeorol.*, 7(3), 548–565.
Walker, J. P., and Houser, P. R. (2001). "A methodology for initializing soil moisture in a global climate model: Assimilation of near-surface soil moisture observations." *J. Geophys. Res.*, 106(D11), 11761–11774.
Wan, E. A., and Van Der Merwe, R. (2000). "The unscented Kalman filter for nonlinear estimation." *Adaptive Systems for Signal Processing, Communications, and Control Symp. 2000. AS-The, SPCC, IEEE 2000*, IEEE, New York.
Wang, D., and Cai, X. (2008). "Robust data assimilation in hydrological modeling—A comparison of Kalman and H-infinity filters." *Adv. Water Resour.*, 31(3), 455–472.
Weerts, A. H., and El Serafy, G. Y. (2006). "Particle filtering and ensemble Kalman filtering for state updating with hydrological conceptual rainfall-runoff models." *Water Resour. Res.*, 42(9), W09403.
Wu, S.-J., Lien, H.-C., Chang, C.-H., and Shen, J.-C. (2012). "Real-time correction of water stage forecast during rainstorm events using combination of forecast errors." *Stochastic Environ. Res. Risk Assess.*, 26(4), 519–531.
Xiong, L., and O'Connor, K. M. (2002). "Comparison of four updating models for real-time river flow forecasting." *Hydrol. Sci. J.*, 47(4), 621–639.
Yu, P.-S., and Chen, S.-T. (2005). "Updating real-time flood forecasting using a fuzzy rule-based model/Mise à Jour de Prévision de Crue en Temps Réel Grâce à un Modèle à Base de Règles Floues." *Hydrol. Sci. J.*, 50(2), 265–278.
Zealand, C. M., Burn, H. D., and Simonovic, S. P. (1999). "Short term streamflow forecasting using artificial neural networks." *J. Hydrol.*, 214(1), 32–48.